Electronic supplementary information

Hydroquinone-treated $Cu_3(BTC)_2$: A mixed-valence Cu(I/II) MOF catalyst for efficient cycloadditions

Sun Ho Park,‡[a] Hye Mi Kim,‡[a] Mariana L. Díaz-Ramírez,‡[ab] Sunggi Lee [*ab] and Nak Cheon Jeong*[ab]

[a]Department of Physics & Chemistry, DGIST, Daegu 42988, Korea
[b]Center for Basic Science, DGIST, Daegu 42988, Korea
‡S.H.P., H.M.K., and M.L.D-R contributed equally to this work.

*To whom correspondence should be addressed: S.L. (sunggi.lee@dgist.ac.kr) & N.C.J. (nc@dgist.ac.kr)

Table of contents

Section S1. Materials and methods

Materials. All reagents were obtained from commercial sources (Sigma Aldrich, Alfa Aesar, or Daejung). Copper (II) nitrate hemipentahydrate [$Cu(NO_3)_2 \cdot 2.5H_2O$, 98.0-102%, Aldrich], trimesic acid (1,3,5-bezenetricarboxylic acid, H_3BTC, 95%, Aldrich), ethanol (EtOH, 94.5%, Daejung), N,N-dimethylformamide (DMF, 99.5%, Daejung), and distilled deionized water (DDW) were used for the synthesis of HKUST-1 powder. Hydroquinone (H_2Q, 99.5%, Aldrich) and anhydrous acetonitrile (MeCN, 99.8%, Aldrich) were used for the H_2Q treatment of HKUST-1. The MeCN was distilled and purified with activated zeolite 4A in a moisture-free argon-filled glove box before use (anhydrous MeCN). Phenylacetylene (98%, Aldrich), 1-Ethynyl-4-fluorobenzene (98%, Fisher), 1-Chloro-4-ethynylbenzene (98%, Aldrich), 1-Bromo-4-ethynylbenzene (98%, TCI), 4-Ethynyltoluene (97%, TCI), 4-Ethynylanisole (98%, TCI), benzyl azide (94%, Alfa), 4-Methylbenzyl bromide (98%, Fisher), 4-Nitrobenzyl bromide (87%, Fisher), 4-Fluorobenzyl bromide (97%, Aldrich), 2-Fluorobenzyl bromide (98%, Fisher), and EtOH were used for the azide-alkyne cycloaddition reaction. Deuterated acetonitrile (MeCN-d_3, 99%, Aldrich) was used for supernatant solution after H_2Q treatment with the ^{1}H-nuclear magnetic resonance (^{1}H NMR) spectroscopic analysis. The deuterated chloroform ($CDCl_3$, 99%, Aldrich) was used for catalytic reaction with the ^{1}H NMR spectroscopic analysis. All synthesized MOFs were stored in a moisture-free argon-filled glove box before use.

Synthesis of HKUST-1. We synthesized HKUST-1 following the procedure described in our previous reports.[1] Briefly, $Cu(NO_3)_2 \cdot 2.5H_2O$ (0.87 g, 3.6 mmol) was dissolved in 10 mL of DDW in a vial. In a separate vial, H_3BTC (0.22 g, 1.0 mmol) was dissolved in 10 mL of EtOH. The $Cu(NO_3)_2$ solution was quickly added to the vial containing the H_3BTC solution. After the mixed solution was continuously stirred for 10 min at room temperature, 1 mL of DMF was added to the mixed solution. Then, the vial was sealed with polytetrafluoroethylene (PTFE) tape. The vial was placed in an oven at 80 °C for 20 h to allow the mixture to react. After the product cooled to room temperature, we collected and washed the crystalline solid (pristine HKUST-1) with a mixed solvent of H_2O and EtOH (0.16 g, 53%).

Thermal activation (TA) of HKUST-1. Coordinated H_2O and EtOH solvents in pristine HKUST-1 were removed by performing the TA before the H_2Q-treatment of HKUST-1 (hereafter, we call H_2Q-treated HKUST-1 as Cu(I/II)-HKUST-1). For the TA of pristine HKUST-1, a pristine HKUST-1 sample was placed in a glass vacuum tube. Then, the tube was heated at 150 °C for 24 h under vacuum conditions (~10^{-3} Torr). After cooling to room temperature, the tubes were transferred into a moisture-free argon-charged glove box. Hereafter, we refer to this thermally activated HKUST-1 as Act-HKUST-1.

H_2Q-treatment of HKUST-1. 0.50 g of Act-HKUST-1 powder was placed in a 20 mL vial. In a separate vial, we placed an H_2Q solution by dissolving 0.137 g of H_2Q in 20 mL of anhydrous MeCN. After the H_2Q solution was added to the vial containing Act-HKUST-1, the vial was placed on a hotplate at 80 °C for 12 h to allow the H_2Q to react with HKUST-1. After the vial cooled down to room temperature, we collected and washed the Cu(I/II)-HKUST-1 crystals with the anhydrous MeCN. Finally, the obtained Cu(I/II)-HKUST-1 crystals were dried under vacuum before use. The entire process was conducted under an inert atmosphere in a moisture-free argon-charged glove box HKUST-1 (0.41 g, 82%).

Azide-alkyne cycloaddition reaction. We prepared a solution containing 0.4 mmol of phenylacetylene (PA) and 0.2 mmol benzyl azide (BA) by dissolving them in 1 mL EtOH using a vial. After 0.007 mmol Cu(I/II)-HKUST-1 catalyst was added to the mixture, the vial was placed in an oil bath and allowed to react at 80 °C for 12 h. We confirmed the reaction products by ^{1}H NMR. Additionally, we extended the experiments to various alkynes and azides with different functional groups under the same conditions. Meanwhile, we also experimented with the reaction conditions by testing the presence or absence of

the catalyst and controlling the reaction time and temperatures for comparison.

Recycle test of Cu(I/II)-HKUST-1 catalyst. After finishing an azide-alkyne cycloaddition reaction, the Cu(I/II)-HKUST-1 powder used as a catalyst was collected via filtration. The collected powder was subsequently washed with EtOH. For TA of Cu(I/II)-HKUST-1, a collected powder was placed in a glass vacuum tube. Then, the tube was heated at 150 °C for 24 h under vacuum (~10^{-3} Torr) conditions. After cooling to room temperature, the tubes were transferred into a moisture-free argon-charged glove box. Eventually, the used Cu(I/II)-HKUST-1 powder was repeatedly tested with the catalytic reactions to check recyclability.

Preparation of Azide (Substrate) with different functional groups.

4-methylbenzyl azide. We synthesized 4-methylbenzyl azide following the procedure described in previous reports.[2] In a 25 mL flask, 4-methylbenzyl bromide (10 mmol) was added to a sodium azide (11 mmol) solution dissolved in 20 mL of DMSO with stirring. The reaction mixture was continuously stirred at 80 °C overnight. After cooling to room temperature, the mixture was diluted with 50 mL of water and extracted three times with 5 mL of diethyl ether. The combined organic layers were washed with brine, dried over $MgSO_4$, and concentrated under reduced pressure. The crude product was obtained with a yield of 80.6%.

4-nitrobenzyl azide. We synthesized 4-nitrobenzyl azide following the procedure described in previous reports.[3] In a 50 mL flask, we dissolved 4-nitrobenzyl bromide (10 mmol) in 20 mL of DMSO. Then, sodium azide (11 mmol) was slowly added to the flask. The reaction mixture was stirred at room temperature for 12 hours. After reaction termination, the reaction was quenched by adding 50 mL of water. The aqueous solution was extracted three times with 50 mL of ethyl acetate, and the combined organic phases were washed 3 times with 50 mL of brine and dried overnight using $MgSO_4$. The mixture was then filtered, and the filtrate was evaporated under low-pressure conditions to yield 4-nitrobenzyl azide (74.9% yield).

4-fluorobenzyl azide.

We synthesized 4-fluorobenzyl azide following the procedure described in previous reports.[4] In a 100 mL glass bottle, we added sodium azide (3.75 mmol) to a 4-fluorobenzyl bromide (2.5 mmol) solution dissolved in 50 mL of water/acetone mixture (1:4). The resulting suspension was continuously stirred at room temperature for 24 hours. After DCM was added to the mixture, the organic layer was separated. The aqueous layer was extracted three times with 10 mL of DCM. The combined organic layers were dried using $MgSO_4$ and concentrated under low-pressure conditions to obtain 4-fluorobenzyl azide (49.1% yield).

2-fluorobenzyl azide.

We synthesized 2-fluorobenzyl azide following the procedure described in previous reports.[5] In a 25 mL flask, we dissolved 2-fluorobenzyl bromide (5.32 mmol) in 10 mL of DMF. Then, sodium azide (6.38 mmol) was added while stirring at room temperature. The reaction mixture was heated at 80 °C for 1 hour, then stirred at room temperature for an additional 3 hours. Afterward, 50 mL of water was added to the mixture, and the product was extracted three times using 50 mL of diethyl ether. The combined organic layers were washed three times with 50mL of brine and dried using $MgSO_4$. Finally, it was concentrated under low-pressure conditions to afford the product to yield (50.7%).

Instrumentation. DDW was obtained from a water purification system (Merck Millipore, MQ Direct 8). Powder X-ray diffraction (PXRD) patterns were obtained using a PANalytical diffractometer (Empyrean) equipped with a monochromatic nickel-filtered Cu Kα beam. ^{1}H-NMR spectra were recorded on an

AVANCE III HD FT-NMR spectrometer (Bruker, 400 MHz for ^{1}H). The ^{1}H chemical shifts were referenced to the residual proton resonance of the solvent. FT-Infrared (IR) absorption spectra were obtained using a Nicolet Continuum instrument from Thermo Scientific. X-ray photoelectron spectroscopy (XPS) analysis was performed using an X-ray photoelectron spectrometer (Thermo Scientific, ESCALAB 250Xi). N_2 adsorption/desorption isotherms were obtained at 77 K in a Belsorp MAX instrument from MicrotracBel Corp. Thermogravimetric analysis (TGA) was performed using Thermobalance Q50 (TA instruments). Inductively coupled plasma optical emission spectroscopic (ICP-OES) analysis was conducted using iCAP7400DUO (Thermo Scientific)

Section S2. Reaction mechanism for electron donation reaction of H_2Q to Cu^{2+}.

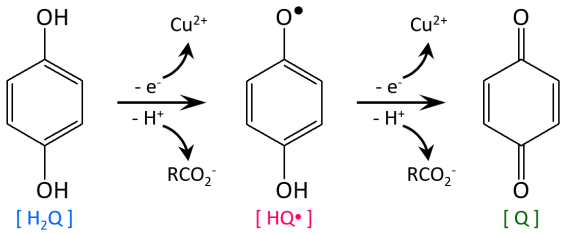

Fig. S1 Illustration of the proposed mechanism for the coordinative reduction of Cu(II) to Cu(I) by hydroquinone (H_2Q). The process involves a two-step proton-coupled electron transfer, resulting in the formation of quinhydron radical (HQ•) and p-benzoquinone (Q). The Cu(II) ions are reduced to Cu(I) during the reaction.

Section S3. Characterization of Cu(I/II)-HKUST-1

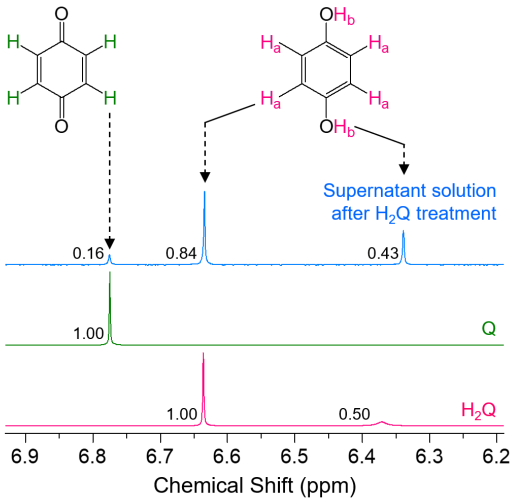

Fig. S2 ^{1}H NMR spectra of a commercial hydroquinone (pink) and benzoquinone (green) dissolved in deuterated MeCN (CD_3CN), alongside a supernatant solution obtained after H_2Q treatment of HKUST-1 (blue). The supernatant solution was diluted in CD_3CN.

An insightful reviewer asked us to demonstrate that coordinative reductions always have the same reduction percentage (33%). To address this question, we have conducted the additional three experiments using the same amount of H_2Q (1:0.5 in the ratio of Cu^{2+}:H_2Q) and three more experiments using the double amount of H_2Q (1:1 in the ratio of Cu^{2+}:H_2Q). In all cases, the results showed that approximately 33% of the total Cu(II) ions were reduced. The reason why only 33% of the Cu(II) ions are reduced is due to the formation of $[Cu(MeCN)_4]^+$ complexes. When Cu^{2+} ions are reduced to Cu^+, some Cu^+ ions dissociate from the framework and form these complexes for overall charge balance, which occupy sodalite-type small octahedral cages within the HKUST-1 framework. However, the number of these cages is limited, allowing only about 16.67% of the Cu(I) to exist as $[Cu(MeCN)_4]^+$ complexes. The remaining 16.67% of Cu(I) ions are located in the paddlewheel node, which plays a role in preserving structural integrity. Consequently, the reduction process stopped at 33% automatically, constrained by the limited number of small cages for placing the complex.

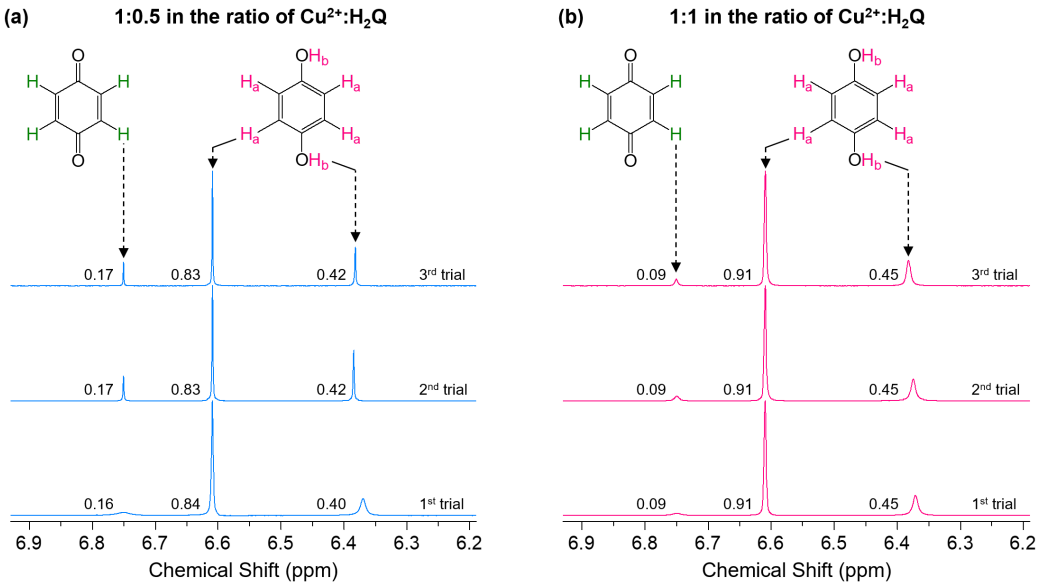

Fig. S3 ^1H NMR spectra of the supernatant solution obtained after H_2Q treatment (a) with1:0.5 and (b) 1:1 in the ratio of Cu^{2+}:H_2Q of HKUST-1. The supernatant solution was diluted in CD_3CN prior to taking NMR spectra.

XPS analysis of hydroquinone-treated HKUST-1 further supports that the treatment leads to the reduction of Cu(II) to Cu(I) and thereby engenders mixed-valenced Cu(I/II)-HKUST-1, showing a band with a shoulder at approximately 933−935 and 952−954 eV, indicative of a mixture of Cu(II) and Cu(I). These main bands are deconvoluted into two components, which correspond to Cu(II) and Cu(I): the bands assigned to Cu(II) appeared at 934.5 and 954.2 eV, while those for Cu(I) appeared at slightly lower binding energies of 933.0 and 952.5 eV. We also examined the XPS analysis with a MeCN coordinated HKUST-1 (MeCN-HKUST-1), which is not treated with H_2Q, for comparison. In contrast to Cu(I/II)-HKUST-1, the MeCN-HKUST-1 sample showed XPS bands corresponding solely to Cu(II) at 934.7 and 954.4 eV, respectively, for Cu 2p3/2 and Cu 2p1/2 transitions, consistent with the Cu(II) bands in Cu(I/II)-HKUST-1.

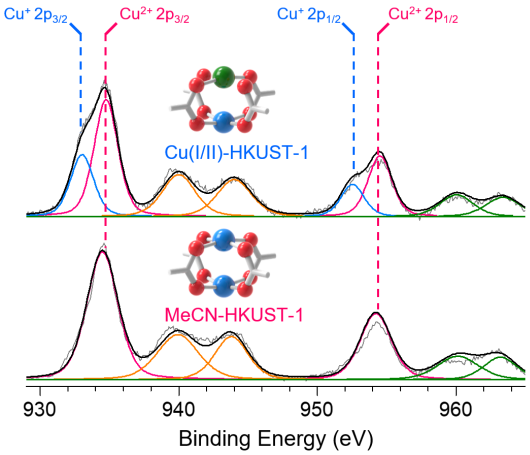

Fig. S4 XPS spectra of Cu(I/II)-HKUST-1 and MeCN-HKUST-1 samples.

Table. S1 Cu 2p bands obtained from XPS spectra for Cu(I/II)-HKUST-1, showing binding energies, full width at half maximum (FWHM), and relative amount of Cu^{2+} and Cu^{+} species.

Signal	Binding Energy (eV)	FWHM (eV)	Percent (%)
Cu^{2+} $2p_{3/2}$	934.5	2.03	66.23
Cu^{+} $2p_{3/2}$	933.0	1.97	33.77

The formation of the $[Cu(MeCN)_4]^+$ complex was confirmed by the FT-IR spectrum of the Cu(I/II)-HKUST-1 sample, which shows the bands at 2275 and 2303 cm^{-1}, corresponding to C≡N vibration modes that agreed well with those of the commercial $[Cu(MeCN)_4]BF_4$ complex. By contrast, the MeCN-HKUST-1 spectrum displayed a band at 2254 cm^{-1} attributed to C≡N vibration and a band at 2293 cm^{-1} attributed to a combination of C–C stretching and C–H bending modes in the MeCN molecules coordinated at the OMSs.[6]

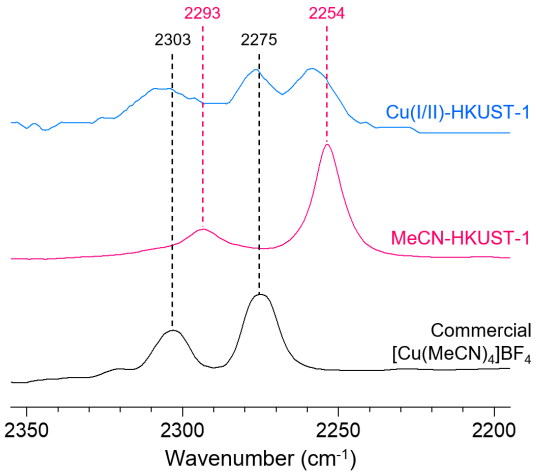

Fig. S5 FT-IR absorption spectra of Cu(I/II)-HKUST-1 (blue), MeCN-HKUST-1 (pink), and commercial $[Cu(MeCN)_4]BF_4$ (black) samples. The spectra highlight the characteristic C≡N stretching vibrations, with Cu(I/II)-HKUST-1 exhibiting peaks at 2305 cm^{-1} and 2275 cm^{-1}, MeCN-HKUST-1 at 2293 cm^{-1} and 2254 cm^{-1}, and the commercial $[Cu(MeCN)_4]BF_4$ at 2303 cm^{-1} and 2275 cm^{-1}.

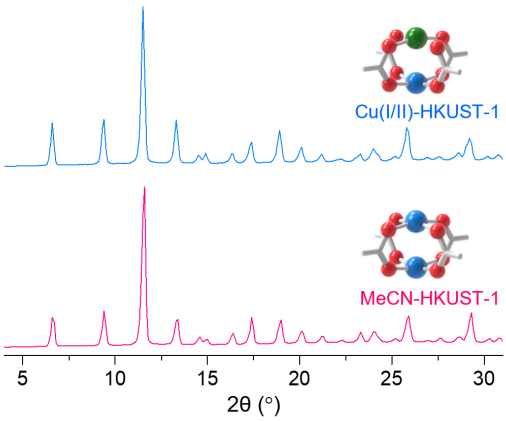

Fig. S6 PXRD patterns of Cu(I/II)-HKUST-1 and MeCN-HKUST-1 samples.

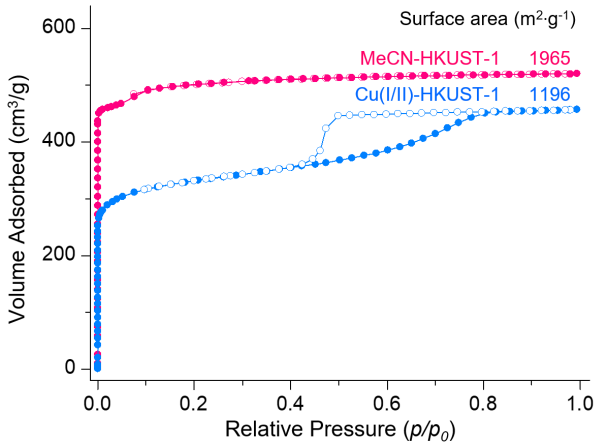

Fig. S7 N_2 adsorption/desorption isotherms of Cu(I/II)-HKUST-1 and MeCN-HKUST-1 samples.

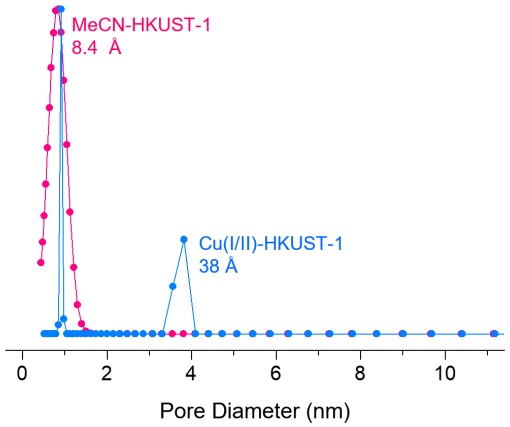

Fig. S8 DFT pore size distributions of Cu(I/II)-HKUST-1 and MeCN-HKUST-1 samples.

A reviewer asked us to show thermogravimetric analysis (TGA) on the samples of pristine HKUST-1 (Pri-HKUST-1) and Cu(I/II)-HKUST-1. The TGA results show that Pri-HKUST-1 starts to decompose at approximately 300 °C, while Cu(I/II)-HKUST-1 begins decomposition at around 280 °C. Although the decomposition temperatures are slightly different between the two due to the low coordination number of Cu(I), the Cu(I/II)-HKUST-1 shows thermal stability comparable to the Pri-HKUST-1. In addition, we observed that the weight loss of Cu(I/II)-HKUST-1 to 280 °C is lower than Pri-HKUST-1, which is seemingly due to the placement of $[Cu(MeCN)_4]^+$ complexes inside the sodalite-type small cages and thereby low water contents in the cages.

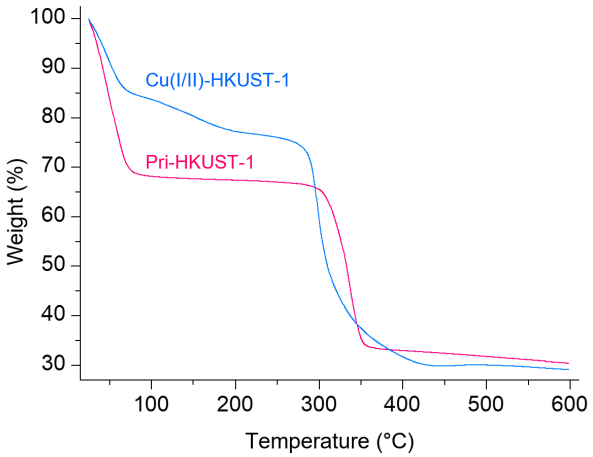

Fig. S9 TGA measurements of Pri-HKUST-1 and Cu(I/II)-HKUST-1.

Section S4. Catalytic activity assessment of the Cu(I/II)-HKUST-1

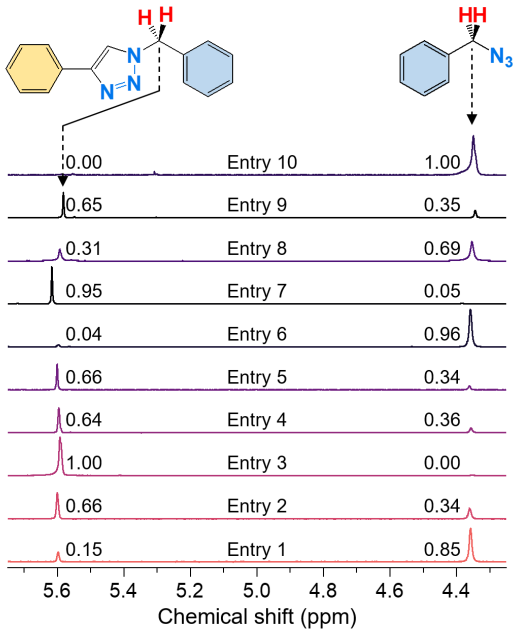

Fig. S10 ^{1}H NMR spectra illustrating the optimization of reaction conditions for the Cu(I/II)-HKUST-1-catalyzed azide-alkyne cycloaddition reaction. The spectra correspond to different entries, showing the relative conversion of reactants to the triazole product. These NMR spectra correspond to Table 1 in the main text.

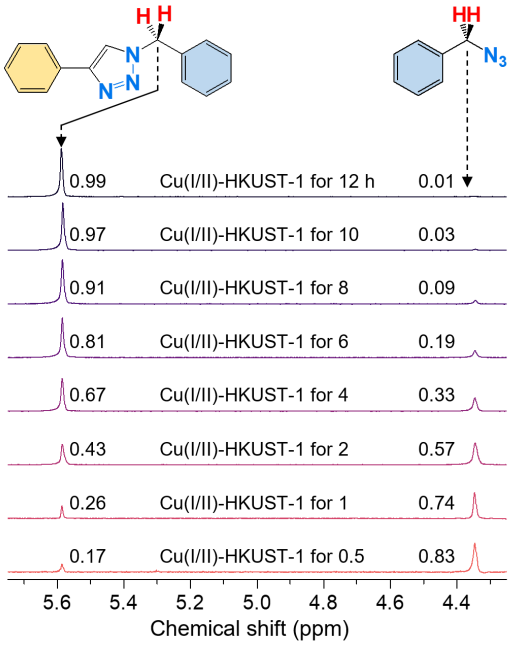

Fig. S11 ^{1}H NMR spectra showing the time-dependent conversion profiles for the azide-alkyne cycloaddition reaction catalyzed by Cu(I/II)-HKUST-1. The spectra correspond to different reaction times, illustrating the gradual conversion of reactants to the triazole product over 12 hours.

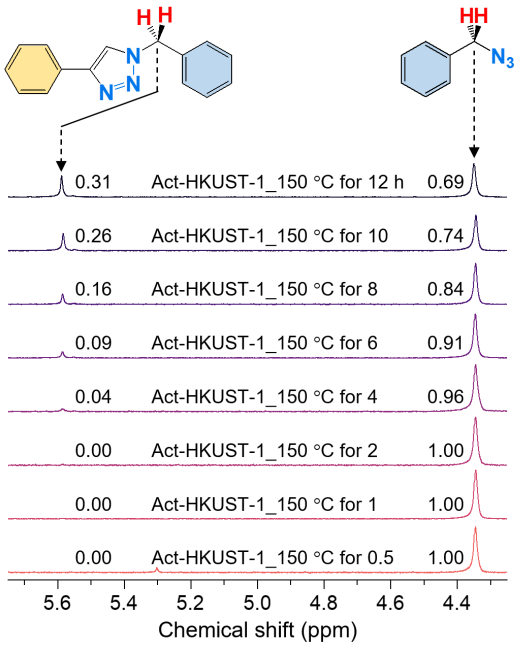

Fig. S12 ^{1}H NMR spectra showing the time-dependent conversion profiles for the azide-alkyne cycloaddition reaction catalyzed by Act-HKUST-1. The spectra correspond to different reaction times, indicating the slower conversion of reactants to the triazole product compared to Cu(I/II)-HKUST-1.

Section S5. Leaching test of Cu(I/II)-HKUST-1 after catalytic reaction

An insightful reviewer asked us whether metal ions are leached during the catalytic reaction. Therefore, we performed a hot filtration experiment and inductively coupled plasma (ICP) analysis. Specifically, we removed the Cu(I/II)-HKUST-1 catalyst 4 hours after the reaction started to observe whether the reaction continued even after the catalyst was removed. As shown in Fig. 2a, after removing the catalyst, the conversion remained unchanged over the subsequent 8 hours. Additionally, ICP results of the supernatant solution performed after the catalytic reaction was terminated showed that only 0.007% of Cu species were detected, indicating that negligible leaching occurred. These results demonstrate that the catalytic reaction is heterogeneous and that the catalyst exhibits high stability during the reaction.

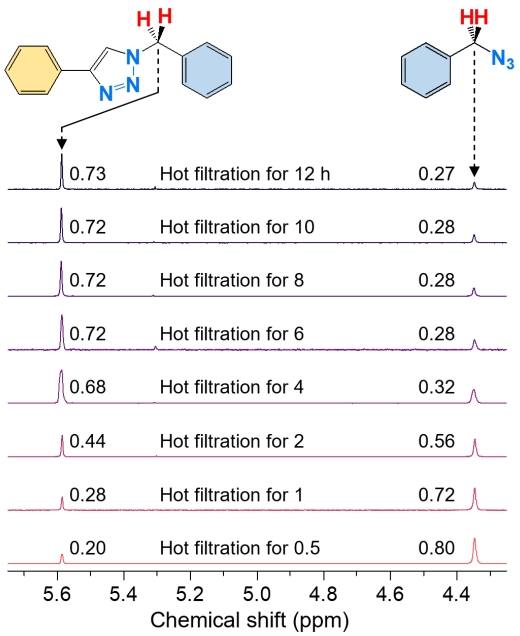

Fig. S13 ^{1}H NMR spectra showing the time-dependent conversion profiles for the hot filtration experiment. The Cu(I/II)-HKUST-1 was removed 4 hours after the reaction started.

Table S2 ICP-OES results of the supernatant solution obtained after the catalytic reaction was terminated.

Term	Calculation	Calculation result
Loading amount of Cu(I/II)-HKUST-1		0.007 mmol
Loading amount of Cu[a]	0.007 mmol x 3	0.021 mmol
Obtained Cu content leached into the supernatant[b]		0.100 ppm
Mass of Cu leached into the supernatant[c]	1 mL x 0.100 mg / 1000 mL	0.0001 mg
Mole of Cu leached into the supernatant	0.0001 mg / 63.546[d] g mol^{-1}	1.574 x 10^{-6} mmol
Mole percent of leached Cu to the total number of Cu	100 * 1.574 x 10^{-6} mmol / 0.021 mmol	0.007 mol%

[a]The chemical formula of HKUST-1 is $Cu_3(C_9H_3O_6)_2$

[b]Value obtained from a ICP-OES analysis

[c]1 mL of solvent was used in the catalytic reaction

[d]Molecular weight of Cu is 63.546 g mol^{-1}

Section S6. Phase integrity of Cu(I/II)-HKUST-1 after catalytic reaction

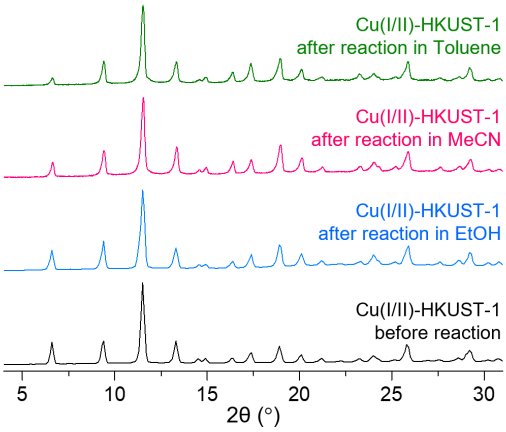

Fig. S14 PXRD patterns of Cu(I/II)-HKUST-1 before (black) and after catalytic reactions in EtOH (blue), MeCN (pink), and Toluene (green).

Section S7. Copper-catalyzed azide-alkyne cycloaddition reaction of various MOFs

An insightful reviewer suggested adding a table summarizing the results of previous studies in order to compare this work. Based on this summary, we found that the catalytic performance of Cu(I/II)-HKUST-1 in the CuAAC reaction is highly comparable to those of MOFs reported recently.

Table S3 Copper-catalyzed azide-alkyne cycloaddition reaction of various MOFs

Catalyst	Loading (mol%)	Temp. (°C)	Time (h)	Yield (%)	Ref.
Cu(I/II)-HKUST-1	3.5	80	12.0	100	This work
Cu_2H_2DOBDC	3.1	80	2.5	99	7
$[2Cu(L)(A)\cdot 3H_2O]_n$	2.0	80	24.0	100	8
$[Cu(CPA)(BDC)]_n$	10.0	70	7.0	93	9
CuBTC–PyDC	5.0	70	3.0	100	10
Fe_3O_4@HKUST-1	1.8	reflux	2.0	92	11
$Cu(INA)_2$-MOF	5.0	80	0.03	98	12
$Cu_3(Br)_3(L)$	0.7	70	8.0	100	13
$[Cu^2(CN)(L)(OCH_3)]\cdot CH_3OH\cdot 3H_2O$	0.7	70	8.0	100	13
$[Cu(H_3L)(\mu_{1,3}\text{-}N_3)(N_3)]_n$	1.1	40	3.5	93	14
$Cu_4(SiW_{12}O_{40})(L)_2(DMF)_2]\cdot 2EtOH\cdot DMF$	0.5	80	12.0	99	15
$[Cu_4Cl_4L]\cdot CH_3OH\cdot 1.5H_2O$	0.8	60	8.0	99	16
$Cu_2(BDC)_2$(DABCO)	7.0	120	1.0	97	17
$[CuI_4(SiW_{12}O_{40})(L)]\cdot 6H_2O\cdot 2DMF$	0.5	80	12.0	99	18
CuI@UiO-67-IM	2.0	80	2.0	89	19
[Cu(i)$_6$I$_6$(Cu(ii)-TPPP)]·2DMF	1.0	50	12.0	100	20
$\{[Cu_6(bpz)_6(CH3CN)_3(CN)_3Br]\cdot 2OH\cdot 14CH_3CN\}_n$	1.0	60	2.0	99	21
$Cu(PTZ)(NSA)_{0.5}\cdot H_2O$	0.3	50	2.5	94	22

Section S8. ^{1}H NMR spectra for the catalytic activity of a Cu(I/II)-HKUST-1 sample over five cycles

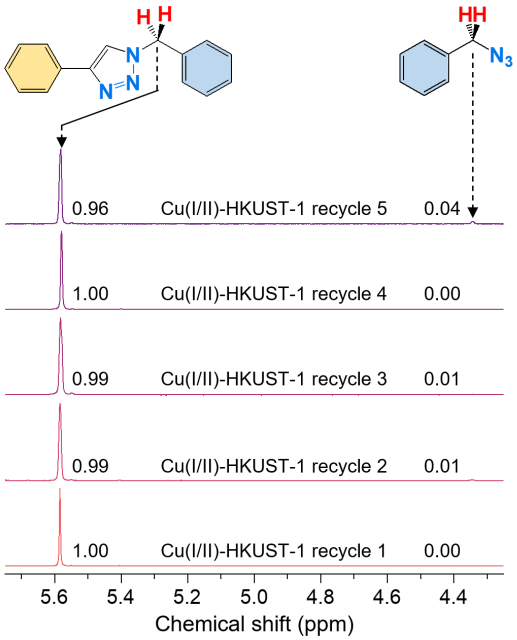

Fig. S15 ^{1}H NMR spectra demonstrating the catalytic recyclability of Cu(I/II)-HKUST-1 over five cycles in the azide-alkyne cycloaddition reaction. The spectra show consistent conversion to the triazole product across all cycles, indicating the catalyst's stability and effectiveness.

Section S9. Phase integrity of Cu(I/II)-HKUST-1 after catalytic reaction over five cycles

An insightful reviewer asked us to add a PXRD analysis of Cu(I/II)-HKUST-1 after each catalytic cycle to demonstrate whether the framework structure remained intact during the cycles. Thus, we have performed the PXRD analysis with the Cu(I/II)-HKUST-1 after each catalytic reaction. As a result, the PXRD patterns demonstrated that the structural integrity of the catalyst is well preserved over the cycles.

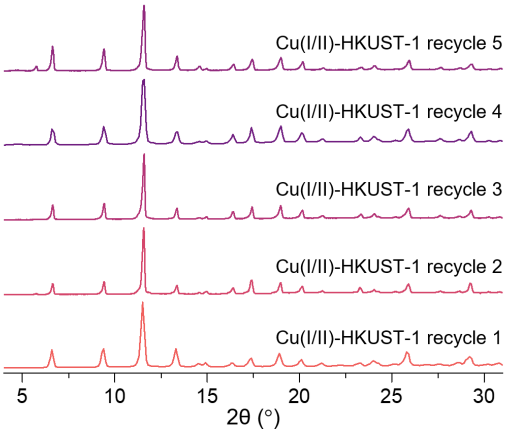

Fig. S16 PXRD patterns of Cu(I/II)-HKUST-1 after the catalytic reactions over five cycles.

Section S10. ^{1}H NMR spectra of substrate scope for Cu(I/II)-HKUST-1 catalyzed azide-alkyne cycloaddition reaction

As suggested by the reviewer, we expanded our catalytic studies to include a broader range of substrates with different functional groups to demonstrate the general applicability of the catalyst. The catalyst exhibited high conversion rates across all tested substrates. Notably, a slightly lower conversion of 84% was observed with 2-fluorobenzyl azide (**1h**), which we attribute to steric hindrance. Thus, these results demonstrate that Cu(I/II)-HKUST-1 is an effective heterogeneous catalyst for a wide range of substrates in the CuAAC reaction.

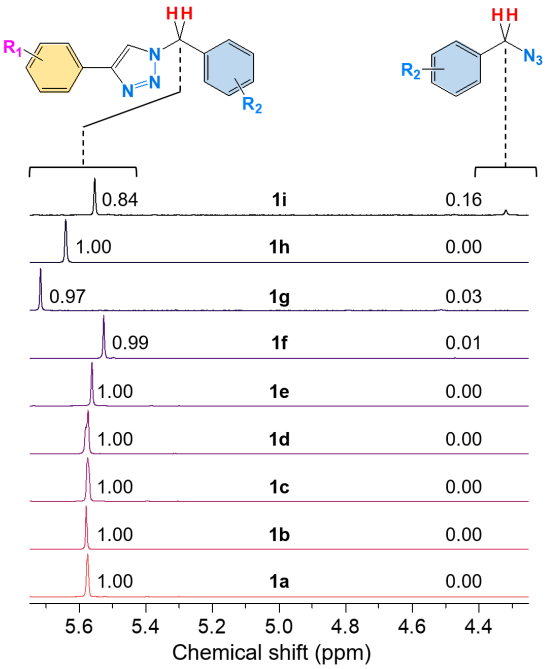

Fig. S17 ^{1}H NMR spectra of various substrate for Cu(I/II)-HKUST-1 catalyzed azide-alkyne cycloaddition reaction.

References

1 D. Song, J. Bae, H. Ji, M.-B. Kim, Y.-S. Bae, K. S. Park, D. Moon and N. C. Jeong, *J. Am. Chem. Soc.*, 2019, **141**, 7853-7864.

2 M. Li, N. Zheng, J. Li, Y. Zheng and W. Song, *Green Chem.*, 2020, **22**, 2394-2398.

3 C. Pardin, I. Roy, W. D. Lubell and J. W. Keillor, *Chem. Biol. Drug Des.*, 2008, **72**, 189-196.

4 L. Campbell-Verduyn, P. H. Elsinga, L. Mirfeizi, R. A. Dierckx and B. L. Feringa, *Org. Biomol. Chem.*, 2008, **6**, 3461-3463.

5 G. Colombano, C. Albani, G. Ottonello, A. Ribeiro, R. Scarpelli, G. Tarozzo, J. Daglian, K.-M. Jung, D. Piomelli and T. Bandiera, *ChemMedChem*, 2015, **10**, 380-395.

6 B. Dereka, N. H. C. Lewis, J. H. Keim, S. A. Snyder and A. Tokmakoff, *J. Phys. Chem. B*, 2022, **126**, 278-291.

7 X. Hou, W. He, X. Zhai, B. Chen, Y. Fu, L. Zhang, J. Chen and Y. Fu, *Inorg. Chem. Front.*, 2024, **11**, 4263-4269.

8 K. Huang, Q. Li, X.-Y. Zhang, D.-B. Qin and B. Zhao, *Cryst. Growth Des.*, 2022, **22**, 6531-6538.

9 K. Naskar, S. Maity, H. S. Maity and C. Sinha, *Molecules*, 2021, **26**, 5296.

10 Z. Fan, Z. Wang, M. Cokoja and R. A. Fischer, *Catalysis Science & Technology*, 2021, **11**, 2396-2402.

11 E. Arefi, A. Khojastehnezhad and A. Shiri, *Sci. Rep.*, 2021, **11**, 20514.

12 J. C. Mansano Willig, G. Granetto, D. Reginato, F. R. Dutra, É. F. Poruczinski, I. M. de Oliveira, H. A. Stefani, S. D. de Campos, É. A. de Campos, F. Manarin and G. V. Botteselle, *RSC Adv.*, 2020, **10**, 3407-3415.

13 J.-F. Li, P. Du, Y.-Y. Liu, G.-H. Xu and J.-F. Ma, *Dalton Trans.*, 2020, **49**, 3715-3722.

14 R. Bikas, F. Ajormal, N. Noshiranzadeh, M. Emami and A. Kozakiewicz, *Appl. Organomet. Chem.*, 2020, **34**, e5826.

15 M.-Y. Yu, T.-T. Guo, X.-C. Shi, J. Yang, X. Xu, J.-F. Ma and Z.-T. Yu, *Inorg. Chem.*, 2019, **58**, 11010-11019.

16 X.-X. Wang, J. Yang, X. Xu and J.-F. Ma, *Chemistry – A European Journal*, 2019, **25**, 16660-16667.

17 H. Tourani, M. R. Naimi-Jamal and M. G. Dekamin, *ChemistrySelect*, 2018, **3**, 8332-8337.

18 B.-B. Lu, J. Yang, G.-B. Che, W.-Y. Pei and J.-F. Ma, *ACS Appl. Mater. Interfaces*, 2018, **10**, 2628-2636.

19 Y.-H. Hu, J.-C. Wang, S. Yang, Y.-A. Li and Y.-B. Dong, *Inorg. Chem.*, 2017, **56**, 8341-8347.

20 W. Jiang, J. Yang, Y.-Y. Liu and J.-F. Ma, *Chem. Commun.*, 2016, **52**, 1373-1376.

21 Z. Xu, L. L. Han, G. L. Zhuang, J. Bai and D. Sun, *Inorg. Chem.*, 2015, **54**, 4737-4743.

22 P. Li, S. Regati, H. Huang, H. D. Arman, J. C. G. Zhao and B. Chen, *Inorg. Chem. Front.*, 2015, **2**, 42-46.